

Influence of Static Magnetic Field on Microstructure and Properties of 7055 Aluminum Alloy

Li Guirong, Cheng Jiangfeng, Wang Hongming, Li Chaoqun

Jiangsu University, Zhenjiang 212013, China

Abstract: The mechanical properties and microstructure of 7055 alloy subjected to static magnetic fields at different magnetic induction intensities ($B=0, 1, 3, 5, 7$ T) were investigated. The dislocation characteristics, phase transition, textures, tensile properties, fracture morphology and residual stress were researched through advanced modern techniques. The results show that the dislocation densities in the treated samples increase with increasing the B , and a transformation of cellular dislocation to the low-energy network dislocation is observed. In addition, the magnetic field also plays a positive role in grain refinement due to the formation of sub-grains, and facilitates the common η (MgZn_2) at grain boundaries to dissolve toward internal grains and to transfer into η' phase, which contributes to the enhancement of the tensile strength and toughness of materials. At $B=3$ T, the magnetic field weakens the lattice distortion and causes a structural adjustment, and material performance reaches an optimal value with an elongation of 10.5%, a residual stress of 38 MPa and a tensile strength of 555 MPa. Besides, the fracture morphologies were analyzed by scanning electronic microscopy, and the fracture characteristics were in agreement with the plasticity property.

Key words: 7055 alloy; dislocation characteristic; microstructure; mechanical properties; static magnetic field

In past decades, with the sustained requirement of new and excellent performance lightweight materials for military and civilian aircraft, aluminum alloys have attracted increasing attention. In particular, 7xxx alloys^[1] have been widely used in the fields of transport, weapons, aerospace and aviation owing to their advanced characteristic of excellent formability, high fracture toughness, well corrosion resistance, welding properties and damage tolerance property^[2-7]. In the 1980s, in order to optimize the composition limits and heat treatment of 7150 aluminum alloy, 7055AA was produced by American Alcoa Company^[8]. Like most age-hardenable alloys, the high strength of 7055AA alloy is attributed to the uniform distribution of coherent GPI, GPII and metastable η' phases. Usually, metastable η' phase is responsible for peak hardening, but the non-coherent η phase leads to the decrease in the strength of 7055Al alloys^[2]. The attractive comprehensive properties of 7055 alloy were achieved by high solute content, high ratio of Zn/Mg and a less content of the impurity of Fe,

Si and Mn. The microstructure, thereafter, was transformed from the saturated solid solution to a super-saturation solid solution, which promoted precipitation-hardening^[9,10]. However, these precipitates were beneficial to the enhancement of strength and intergranular corrosion resistance but deteriorated the plasticity of materials because of the pinning effect of precipitated particles^[11]. Therefore, it is urgent to explore a new approach to overcome these shortcomings and to meet the increasing demand of modern technology.

Recently, there are increasing concerns in the preparation of metallic materials with the aid of magnetic field treatment. It is well known that magnetic fields have a great effect on recrystallization, grain growth, crystal morphology, composition homogenization, phase transition, texture formation and so on^[12-15]. And it has received increasing attention because of its application in materials science^[15,16]. However, the non-magnetic solid materials such as aluminum,

Received date: April 22, 2018

Foundation item: National Natural Science Foundation of China (51371091, 51174099, 51001054); Scientific Research Project of Jiangsu University (15A368); Innovation Funds for Postgraduate of Jiangsu University (SJLX16_0445)

Corresponding author: Li Guirong, Ph. D., Professor, School of Material Science and Engineering, Jiangsu University, Zhenjiang 212013, P. R. China, E-mail: liguirong@ujs.edu.cn

Copyright © 2019, Northwest Institute for Nonferrous Metal Research. Published by Science Press. All rights reserved.

magnesium and titanium alloy treated by magnetic fields, have been scarcely reported. So far, some available reports have been made on the influence of magnetic fields on the dislocation characteristics, and it is believed that the magnetic field can promote the dislocation multiplication and improve the dislocation flexibility, which corresponds to the improvement in the plastic deformation [10,17-22]. In this paper, based on magnetoplasticity effect, 7055Al alloy treated by static magnetic fields was selected to entirely explore the influence mechanism of magnetic field, and thereby to develop and optimize the magnetic theory of plasticity.

1 Experiment

The commercial 7055 aluminum alloy was processed as a standard tensile sample whose chemical composition is listed in Table 1. After homogeneous treatment at 450 °C for 24 h, the billet was squeezed to $\Phi 25$ bar, and the extrusion ratio was 16:1. It was then heat treated in the SX2-5-12 box resistance furnace. The heat treatments are 475 °C/2 h solid solution treatment and aging treatment at 120 °C for 24 h. The microstructure of the experimental materials was a supersaturated solid solution. The dissolved alloy elements were mainly η ($MgZn_2$), S (Al_2CuMg), and T ($AlZnMgCu$) phases separated out in the aging process.

Fig.1 shows the distribution of precipitates in 7055 aluminum alloy. It can be seen that the microstructure includes intracrystalline precipitate, grain boundary precipitate and grain boundary precipitate free zone. Grain boundary precipitate has less influence on strength, but can improve the toughness by preventing the hydrogen diffusion. It is usually suggested that the grain boundary precipitate free zone has no effect on the properties [23]. However, there are a large number of small precipitation phases in grains, and they have a positive effect on tensile strength of materials but reduce the plastic deformation ability due to the pinning effect of precipitates [24].

Table 1 Chemical composition of 7055 aluminum alloy (wt%)

Zn	Mg	Cu	Zr	Ti	Cr	Fe	Si	Mn	Al
8.25	2.1	2.24	0.17	0.06	0.03	0.13	0.09	0.04	Bal.

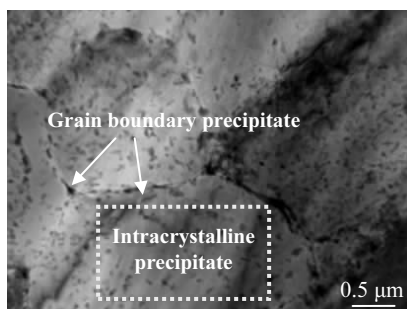


Fig.1 Distribution of precipitates in 7055 aluminum alloy

In the experiment, the samples were exposed to static magnetic fields with $B=0, 1, 3, 5, 7$ T, and the total processing time was set as 200 s. Fig.2a illustrates the schematic diagram of experimental condition, demonstrating the sample status and the relationship between samples and magnetic fields. The microstructures of two flake samples with a size of $\Phi 10$ mm \times 1 mm in the lower position were observed, and the size of tensile sample in the upper position was marked in Fig.2b.

JEOL-JSM-7001F scanning electronic microscopy (SEM) and JEM-2100 transmission electronic microscopy (TEM) were used separately to observe the fracture morphology, precipitates and dislocation characteristics including morphology and distribution. Aiming to avoid the possible interference of the extra stress during the TEM sample processing, an assisted approach was introduced to obtain the dislocation density; By the X-350, a type of X-ray stress meter, the parameter of full width at half maximum (FWHM) can be acquired directly, which was a middle parameter to calculate the dislocation density. The mechanical property of 140 mm tensile sample was tested by DNS10 electro-mechanical universal testing machines so as to explore the effect of static magnetic fields on the performance of 2024 alloy.

2 Results and Discussion

2.1 Effect on microstructure

2.1.1 Dislocation morphology

Fig.3 illustrates the dislocation morphology of samples subjected to different treatments. From Fig.3a, it is evident that the dislocations distribute unevenly in the untreated sample, and the microstructure exhibits a cellular substructure. Besides, the density of intracellular dislocations is low and the dislocations mainly tangle in the cell wall [25]. However, when the samples are exposed to a static magnetic field, the internal dislocations start to loose, and then move toward the cell wall

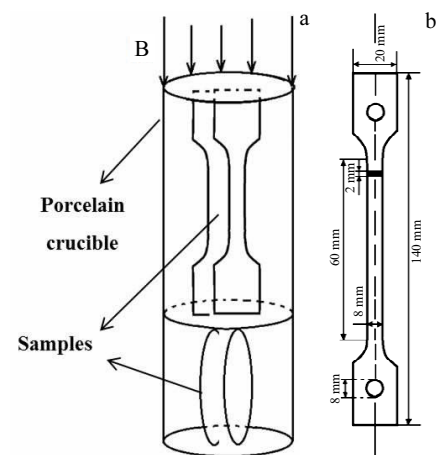


Fig.2 Schematic diagram of experimental condition (a) and size of tensile sample (b)

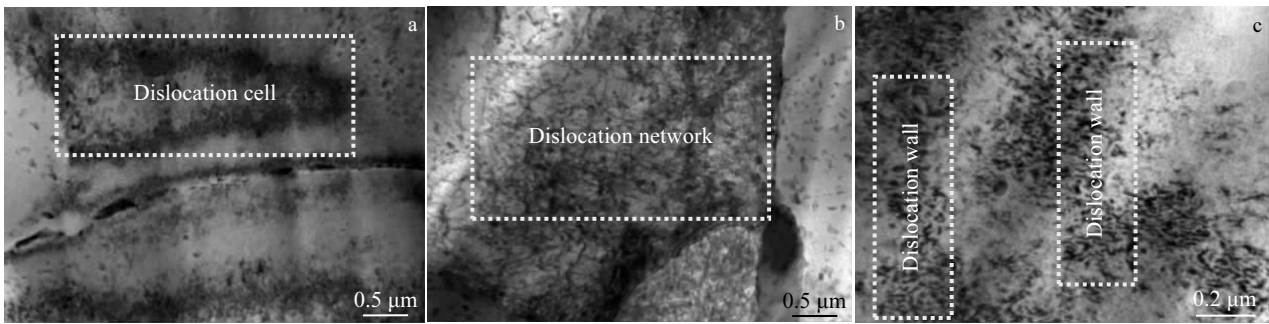


Fig.3 Deformed substructures in static magnetic field: (a) untreated sample, (b) network dislocation after MF treatment, and (c) dislocation wall after MF treatment

by surmounting the low barrier. Due to the interaction between the interior dislocations and the cell wall, the dislocations tend to be in order and form a network structure (Fig.3b). With the further development of net dislocations and the enhancement of dislocation density, the adjacent net dislocations will connect gradually to form the dislocation wall (Fig.3c).

From the atomic scale analysis, the ordered dislocations are due to the rearrangement of atoms under the magnetic fields. The combination and migration of atoms are caused by the electron movement, which depends on whether there is a hole. Atoms in the crystal structure can form chemical bonds with holes. In the absence of holes, the electron pairs of the formed chemical bonds exhibit a reversed spin, which is in a state of spin prohibition and is difficult to be transformed from S to T state^[20,26]. However, in the presence of holes, different bands appear instead of forbidden bands. Under magnetic fields, the

original reversed spin electrons in the forbidden zone will be transformed into homonymous spin, resulting in an empty orbit, and then the original state is destroyed. Subsequently, a new conduction band appears in the combine area, which improves the atomic motion ability. Meanwhile, the electrons will flow in the opposite direction of magnetic field, which promotes the atomic migration.

From the dislocation morphologies shown in Fig.4a, it is apparent that there are dislocation lines and dislocation rings in the initial sample, and the dislocations are in an entangled state, which is not an ideal state for improving the composite properties of materials. In the presence of a static magnetic field, the stacking dislocations can absorb enough energy and gradually form the dislocation walls by climbing, interleaving and rearranging. When $B=1$ T, it is indicated that the dislocation walls have not yet formed, exhibiting discontinuous short term structure, and the dislocations show obvious sparse and

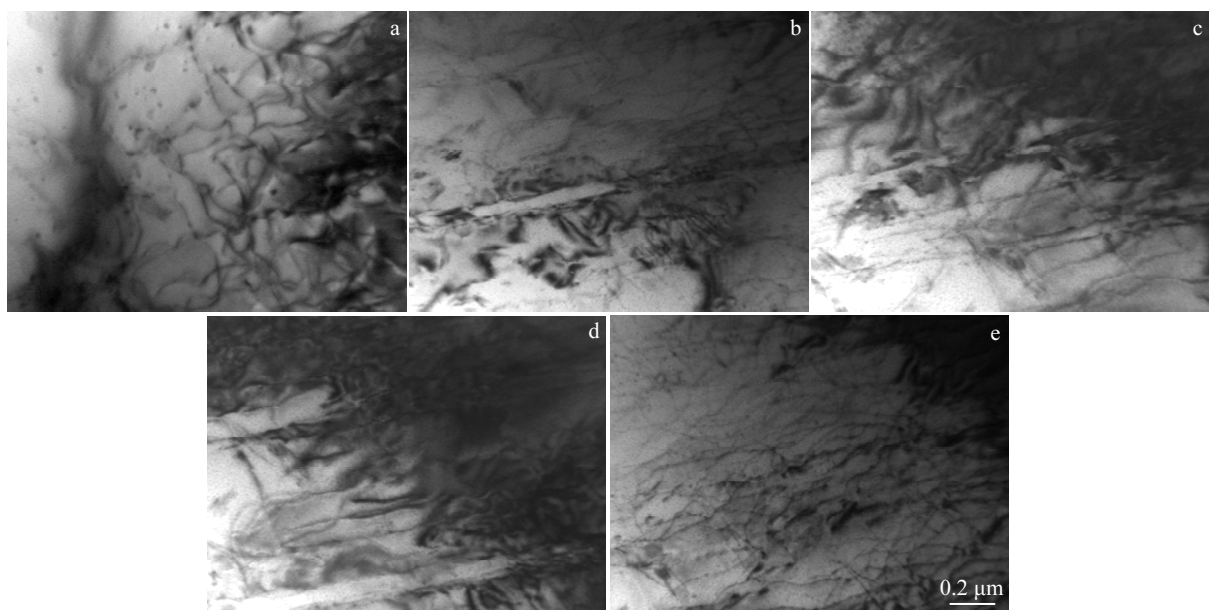


Fig.4 Variation of dislocation morphologies in different static magnetic fields: (a) $B=0$ T, (b) $B=1$ T, (c) $B=3$ T, (d) $B=5$ T, and (e) $B=7$ T

concentration areas. It can also be seen that there are ordered dislocation lines on the edge of sparse and concentration areas, and the dislocations tend to be well-aligned primarily. At $B=3$ T, the dislocation walls are formed, and the density of sparse areas is further decreased while the concentration increases, and the distribution of the dislocations is more ordered (Fig.4c). As the B further increases, at $B=5$ T, it exhibits two states of dislocation walls and dislocation lines. Nevertheless, compared with $B=3$ T, it can be seen that there is a certain increase in the density of sparse areas. The dislocation lines of the sparse areas and the dislocation walls of the dense areas appear successively, and the dislocation distribution is further in order. From Fig.4e, at $B=7$ T, the dislocations can not only depin from the pinning center, but also have the ability to move flexibly and to multiply largely. Even if there are lots of linear dislocations, they pile up again and the dislocation structure tends to be deteriorated.

2.1.2 Dislocation density

The physical parameter of FWHM (l) in X-ray test was introduced to quantitatively characterize the dislocation density (D). Dunn formula (Eq.(1)) is introduced here to reveal the relationship between l and D ^[27].

$$D = \frac{l^2}{4.35b^2} \quad (1)$$

where b is the Burgles vector. Fig.5 summarizes the dependence of l^2 on the B . It reveals that l^2 is in a linear relationship with the dislocation density.

In comparison to the initial sample, it is apparent that the dislocation density decreases in the presence of a static magnetic field. However, it increases as B rises from 1 T to 7 T. From the microstructure diagram, there are plenty of dislocations in the original sample, and the tangled dislocations constitute the border of the cellular substructure. As $B=1$ T, the dislocations started to loosen and intracellular dislocations moved to the cell wall. In the process of sliding and climbing, the reduction of the dislocation densities was mainly due to the counteraction of the unlike dislocations.

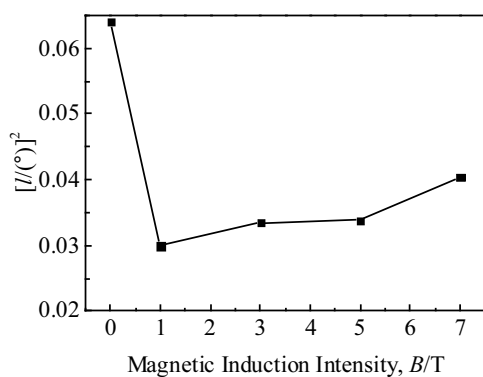


Fig.5 Variation of l^2 with B in static magnetic field

Subsequently, the dislocation density increased with increasing the B , suggesting that the movable dislocations increase, so did the same dislocations during moving. At $B=3$ T, the net dislocations achieved the optimal state. However, in the range of 3 T to 7 T, the moving dislocations were stopped by the strong obstacles and were hard to move further; they started to assemble and presented a disorder and piled up state again, which led to the reduction in the composite properties of materials.

2.1.3 Alloy phase and grain size characteristics

The microstructure characteristics of alloys at different magnetic field intensities are shown in Fig.6. In Fig.6a, the equilibrium phases in the original sample are α phase, short rod and dot precipitated phase, which are typically regarded as squeezed state microstructures. Grains stretch along the rolling direction with a zonal distribution, and some fine grains are clearly visible at the edge of the grain boundary, which are generated by the recovery and recrystallization due to the deformation. There are lots of S (Al_2CuMg), T ($AlZnMgCu$), and undissolved $AlMnFeSi$ phases (black after corrosion) in the grains; these precipitates gathered in the substrate and split it, which resulted in stress concentration around the precipitates. When exposed to external stress, the precipitates tend to be a crack source and a corrosion spot, which are detrimental to the composite properties of materials.

While $B=1$ T (Fig.6b), the zonal structure vanished, and the undissolved phases and impurities decreased, which were evenly distributed in α substrate and weakened the stress concentration. The decrease in undissolved phases and impurities was due to the particles that dissolved into the matrix again. The shapes of the grains were transformed from thick strips into the blocks, and some fine equiaxed grains could be seen in the materials. The change in grain shape is attributed to the fact that the dislocation walls can form the grain boundaries. With the connection of sub-grain boundaries, they can form a new small grain, so the material microstructure overall presented grain refinement.

In Fig.6c, at $B=3$ T, the phase with poor solubility and impurities mainly distributes in punctiform, the quantity of recrystallized grains continues to increase, and the distribution is more homogeneous; meanwhile, the material organization is relatively ideal.

With the enhancement of B , at $B=5$ T (Fig.6d) and $B=7$ T (Fig.6e), even though there are still recrystallized grains, in comparison to the samples of $B=1$ T and $B=3$ T, it can be seen that the sizes of the recrystallization grains decrease obviously, and the grains are difficult to grow up and distribute unevenly. Meanwhile, some solid solution phases separated out and gathered again, resulting in larger precipitates and worse distribution, which would become pinning obstacles to hinder the dislocation motion, and then deteriorate the strength and toughness of materials.

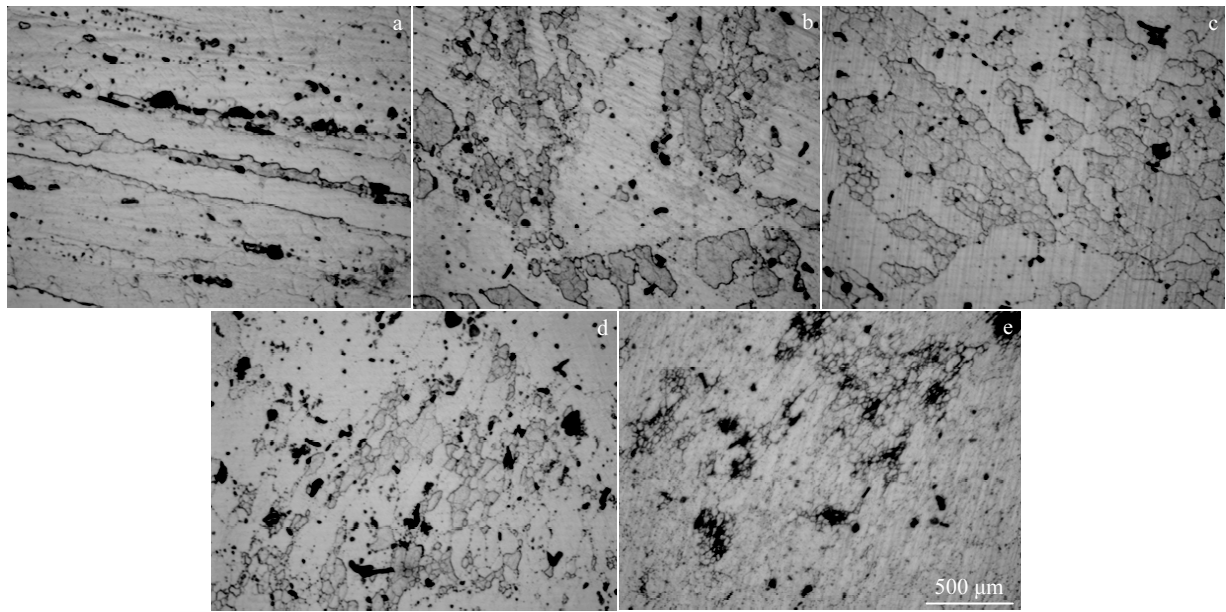


Fig.6 Evolution of grains and precipitates in static magnetic field: (a) $B=0$ T, (b) $B=1$ T, (c) $B=3$ T, (d) $B=5$ T, and (e) $B=7$ T

2.1.4 Phase transition

Fig.7 illustrates the morphology and distribution of precipitates in 7055Al alloy in the original state and at $B=3$ T. It is evident from Fig.7a that there are fine precipitates inside the crystal and bulky precipitates with chain distribution at grain boundaries, which are the typical peak aging process products. In the aging process, solute atoms gathered toward the grain boundaries and caused the precipitates to separate from chain

distribution along grain boundaries, which has little influence on the strength of materials [23], but can improve the stress corrosion cracking resistance [28]. And the bulky precipitates can absorb hydrogen atom, which can prevent hydrogen from diffusing along grain boundary to the crack tip and crack growth. Even if it avoids hydrogen embrittlement and reduces the potential difference between grain boundaries and grains, it also brings about stress concentration at grain boundaries, which easily causes the intergranular fracture and is detrimental to the toughness of the material.

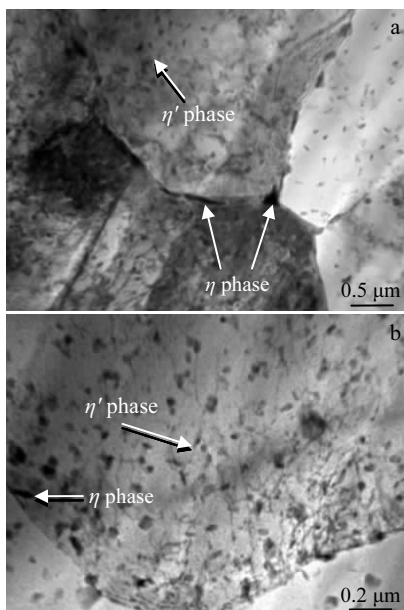


Fig.7 Phase change in static magnetic field: (a) initial state and (b) $B=3$ T

In the static magnetic field at $B=3$ T (Fig.7b), η phase tends to dissolve evenly in the matrix [29]. Because there are numerous solute atoms which are hard to dissolve at the grain boundary, there are still some η phases at the grain boundaries. After magnetic field treatment, solute atoms would separate out again, and η' phase is mainly inside the crystal while η phase is at the boundaries; they distribute closely and are finer than original chain structure (Fig.8c).

From the point of intragranular precipitate characters, magnetic fields changed the characteristics of electronic

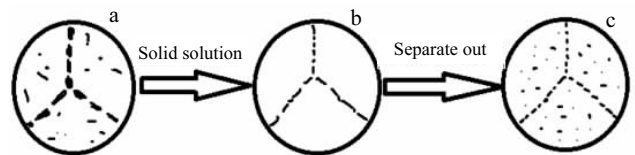


Fig.8 Precipitate redistribution in static magnetic field: (a) untreated sample, (b) η phase after solution treatment, and (c) re-precipitation of intragranular phase

structure and promoted the changes of intragranular precipitate sorts to improve material performance. In the presence of a magnetic field, atoms have a certain ability to diffuse, and some solute atoms might separate or combine and then result in a phase transition. From the quantum scale, electronic state is not stable under magnetic fields. The electrons with high energy would spin the polarization from the single state to the triple state instead of flowing into the defect stably and coupling with electrons in defect.

Under the condition of no spin polarization, the Zn atom and Mg atom of $MgZn_2$ (η) tend to form a strong covalent bond, and the electrons of Mg immigrate toward zinc and easily form $MgZn_2$ (η) phase. However, in the presence of spin polarization, Zn and Mg can form weak covalent bonds instead of strong bonds, which facilitates the generation of instable η' phase. Because of the semi-coherent relationship between η' phase and the aluminum matrix, to a certain extent, it improves the degree of atomic stagger and composite properties of 7055Al alloy [2,30].

Due to the concentration difference, η phases at boundaries dissolve into the crystal while the intragranular η phases dissolve into the matrix. Because of the incoherent relationship between η and aluminum matrix and the semi-coherent relationship between η' phase and the matrix, the η phase transfers into η' phase, which weakens the degree of atomic stagger and decreases the number of η phase which can pin dislocations and weaken the boundary energy. Therefore, dislocations can step over the grain boundaries and move toward the sparse areas, which facilitates the homogeneous distribution of dislocations.

Hence, in the presence of static magnetic fields, η' phase that is partially coherent with the matrix is formed in the crystal, while small and compact incoherent precipitates appear at the grain boundaries, which not only improves the strength, but also increases the toughness and stress corrosion resistance due to the uniform precipitates and various lattice relationships.

2.1.5 Tissue texture

X-ray diffraction analysis of samples subjected to different static magnetic field treatment and the variation of diffraction peaks under different B are presented in Table 2 and Fig.9, respectively. With the assistance of Jade 6.0, the feature graphs of aluminum matrix were selected for analysis. In Table 2, I is

the diffraction peak intensity, $I\%$ is the relative intensity of diffraction peaks and FWHM is the full width at half maximum. It can be seen that the preferred orientation of the initial sample is mainly (220), while the diffraction peak intensity of crystal face (111), (200) and (311) is no more than 10%.

Under the action of static magnetic fields, grain orientation tends to transfer toward (111) and (200). In comparison to the untreated samples, diffraction peak intensities of the samples after magnetic field treatment have a certain increase. As $B=7$ T, diffraction peak intensity of (200) decreased while that of (111) increased abnormally. At this moment, the increase in internal stress and abnormal microstructure cause the crystal orientation bias toward (111). However, as $B=3$ T, the diffraction peak intensities of face (111) and (200) are relatively homogeneous, the deformation in materials tends to be normal, and the lattice distortion as well as preferred orientation are weakened.

2.2 Effect on mechanical properties

2.2.1 Tensile properties

Fig.10 demonstrates the stress-strain curves of the alloy that was tested at different B values. It is apparent that the magnetic fields have a significant effect on the tensile properties of materials when B changes. And the tensile properties of 7055 aluminum alloy after static magnetic fields treatment are given in Table 3.

Fig.11 shows the tendency of tensile strength and elongation of 7055 alloy subjected to different B . The results reveal that the tensile strength decreases with the enhancement of B . When $B \leq 5$ T, the decrease is not obvious, but it is sharp at $B=7$ T. As $B=5$ T, a tensile strength of 545 MPa is obtained, which is decreased by 3.5% compared to that of the untreated sample. However, it is just 490 MPa when $B=7$ T, decreased by 13.3%.

As for elongation, it first rises and then falls as B increases, and when $B=3$ T, the elongation δ reaches 10.5%, which is 40% higher than 7.5% of the initial sample, and the relevant tensile strength is 555 MPa, decreased by 1.8%. As a whole, when B is not more than 3 T, the elongation increases substantially with increasing the B , while the strength decreases slightly, and at $B=3$ T, the material performance achieves the optimal value. It is analyzed that the static magnetic field with a smaller B has a positive effect on

Table 2 X-ray diffraction analysis of sample subjected to static magnetic field treatment

B/T	(111)			(200)			(220)			(311)		
	I	$I\%$	FWHM/(°)									
0	742	9.9	0.316	567	7.5	0.287	7511	100	0.253	143	1.9	0.363
1	19859	100	0.173	11742	59.1	0.194	35	0.2	0.347	238	1.2	0.309
3	12631	100	0.183	9622	76.2	0.214	43	0.3	0.251	197	1.6	0.452
5	15174	100	0.184	11133	73.4	0.196	0	0		199	1.3	0.312
7	70727	100	0.200	20584	29.1	0.230	33	0	0.442	541	0.8	0.334

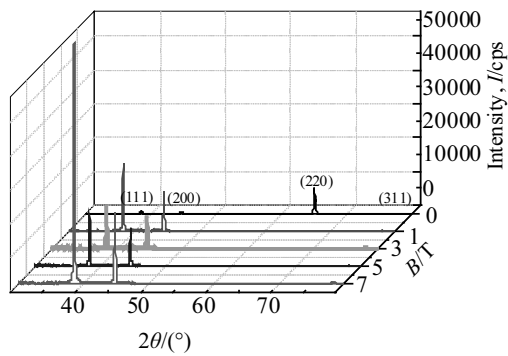


Fig.9 Variation of XRD peaks at different magnetic induction intensities

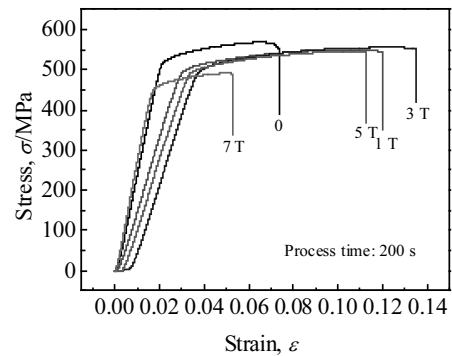


Fig.10 Stress-strain curves at different magnetic induction intensities

Table 3 Tensile properties of 7055 aluminum alloy after static magnetic field treatment

B/T	Tensile strength, σ_b /MPa	Amplification/%	Yield strength, σ_s /MPa	Amplification/%	Elongation, δ /%	Amplification/%
0	565	-	520	-	7.5	-
1	550	-2.7	495	-4.8	9.0	20
3	555	-1.8	498	-4.2	10.5	40
5	545	-3.5	490	-5.8	8.3	10.7
7	490	-13.3	450	-13.5	5.5	-26.7

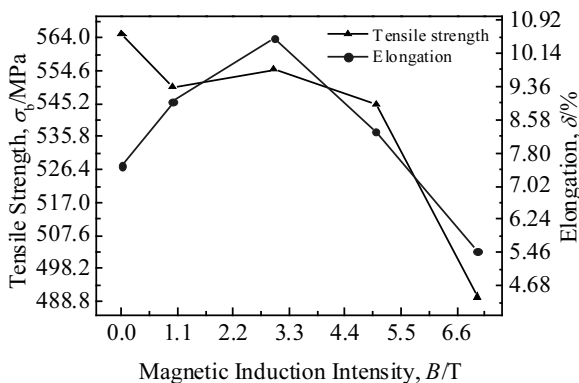


Fig.11 Variation of tensile strength and elongation with magnetic induction density

7055Al alloy, which is termed the positive magneto-plastic effect; however, it shows the negative magneto-plastic effect when B exceeds 3 T.

Combined with the analysis of microstructure characteristics, variation of mechanical performance can be suggested by the following points:

(a) In terms of the dislocation morphology, the dislocations of the initial samples are mainly convolved at the wall of cell substructure, which is not beneficial for the improvement of elongation. As $B=3$ T, due to the dislocation walls and lines caused by dislocation climbing, interleaving and rearranging, the distribution tends to be in order for plastic enhancement.

(b) The decrease in tensile strength is a result of the dislocation density reduction, which is caused by static magnetic fields.

(c) From the morphological features, it can be analyzed that the larger particle precipitates disperse the matrix, and grains exhibit a banding distribution. When $B=3$ T, part of precipitates dissolve into the matrix with uniform dot distribution, and the recrystallized grains have a certain extent of growth and are equiaxed, which is beneficial for the improvement of the toughness of the materials.

(d) From the texture evolution of the original sample, it can be seen that plane (220) is not the sliding direction. In the presence of a static magnetic field, especially $B=1, 3, 5$ T, the grain orientation transfers toward (111) and (200) planes, which contributes to the improvement in elongation as a beneficial sliding plane.

2.2.2 Fracture morphology

Fig.12 indicates the fracture morphologies of samples subjected to different B . It can be seen from Fig.12a that the tensile fracture of the untreated sample exhibits a mixed fracture with dimples and river shape pattern, and there are a large number of precipitates on the bright river shape pattern. During the tensile process, when the stress surrounding the precipitates reaches a certain degree, it will lead to micropores that are caused by the tear of interface between precipitates and matrix or the snap of precipitates, which will expand to fracture. However, in the presence of static magnetic fields, the transition of precipitates and the homogenization of dislocation accelerate the release of internal stress.

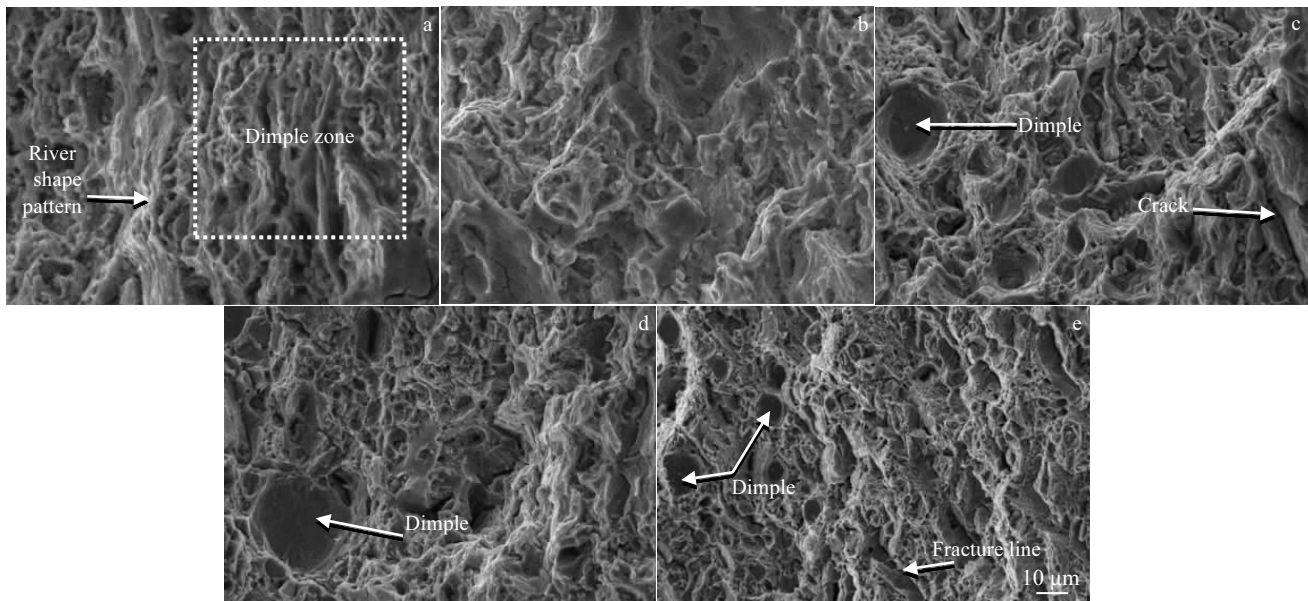


Fig.12 Fracture morphologies of tensile specimen subjected to different static magnetic field treatments: (a) $B=0$ T, (b) $B=1$ T, (c) $B=3$ T, (d) $B=5$ T, and (e) $B=7$ T

Compared with the initial samples, samples at $B=1$ T (Fig.12b) show the color of morphology is dimly and surface relief is obvious, which implies an improvement in the deformability. In Fig.12c, at $B=3$ T, it should be noted that the dimples increase obviously and distribute evenly. When B increased to 5 T, the fracture surface in Fig.12d started to level off, and at $B=7$ T (Fig.12e), the fracture surface appeared with obvious fracture lines and less dimples. Compared with the smaller B treated samples, the tendency of brittle fracture is more outstanding.

2.2.3 Residual stress

Table 4 indicates the residual stress of 7055Al alloy after static magnetic field treatment, and the influence of the magnetic field on the internal residual stress is shown in Fig.13. It can be seen that the residual stress falls first and rises later as B increases, and the minimum value of 38 MPa was obtained at $B=3$ T, representing a decrease of 68.9% compared with the untreated one of 122 MPa.

The residual stress in the material is mainly related to the uniformity of material composition and microstructure distortion, which result in macro and micro internal stresses,

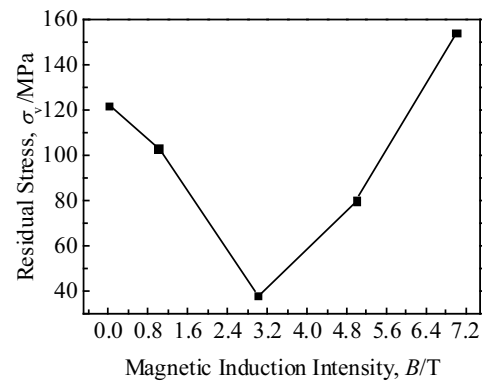


Fig.13 Dependence of residual stress on the magnetic induction density

respectively. Under a static magnetic field, the particle phase (such as η) gathered at grain boundaries would dissolve into crystal to reduce the concentration difference and to decrease the precipitates size, and then decrease the macro residual stress. Meanwhile, because the η phase that is incoherent with the matrix was transformed to η' that is semi-coherent with the matrix, the lattice distortion and micro stress are weakened. On the other hand, the piling up of dislocations can also cause stress concentration (Fig.14), and the rearrangement of dislocation core atoms could decrease the dislocation density and make it tend to be ordered during the movement, weakening lattice distortion and forming the dislocation network and wall, which reduced the stress concentration in a certain extent.

Table 4 Residual stress of 7055 aluminum alloy after static magnetic field treatment

B/T	Residual stress, σ_v /MPa	Amplification/%
0	122	-
1	103	-15.6
3	38	-68.9
5	80	-34.4
7	154	26.6

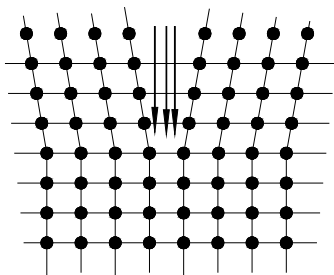


Fig.14 Stress concentration in front of dislocation pile-up

Therefore, the main factors resulting in the reduction of residual stress in the presence of static magnetic fields are the normal lattice distortion, enhanced dislocation mobility, and uniform microstructure. Multilateral dislocation and normal lattice distortion reduced the microscopic stress. Magnetic fields led to the uniform microstructure and refinement of grain boundary chain precipitates, which decreased macroscopic stress, and then improved the plastic deformation ability.

3 Conclusions

1) The static magnetic field can lead to the transition of electron pairs formed between dislocations and obstacles from a single state to a triple state, which facilitates the depinning of dislocation and improves the elongation of the materials. And the cellular dislocations can be transferred to the low-energy network dislocations, and then form the boundaries of sub-grain by migration and merging, which plays an important role in grain refinement.

2) Due to the transition of electron spin under static magnetic fields, the covalent bond between Zn and Mg is broken and a weak bond is reformed, which facilitates the transition from η phase to η' phase, thereby improving the properties of the materials.

3) In comparison to the initial sample, crystal of the sample after magnetic field treatment tends to deform along an advantage slip direction. As $B=3$ T, the lattice distortion is weakened, indicating that the magnetic fields adjust the material structure. At the same time, the material performance reaches the optimal value. The elongation is 10.5%, increased by 40%, while the tensile strength is 555 MPa, and the residual stress is 38 MPa, decreased by 1.8% and 68.9%, respectively.

References

- 1 She H, Shua D, Wang J et al. *Materials Characterization*[J], 2016, 113: 189
- 2 Schreiber J M, Omcikuz Z R, Eden T J et al. *Journal of Alloys and Compounds*[J], 2014, 617: 135
- 3 Sharma M M, Amateau M F, Eden T J. *Acta Materialia*[J], 2010, 58(6): 2292
- 4 Liu S D, Li C B, Han S Q et al. *Journal of Alloys and Compounds*[J], 2015, 625(15): 34
- 5 Rometsch P A, Zhang Y, Knight S. *Transactions of Nonferrous Metals Society of China*[J], 2014, 24(7): 2003
- 6 Yan Liangming, Shen Jian, Li Zhoubing et al. *Transactions of Nonferrous Metals Society of China*[J], 2013, 23(3): 625
- 7 Zhou Song, Wang Lei, Xie Liyang et al. *Transactions of Nonferrous Metals Society of China*[J], 2016, 26: 938
- 8 Yu Hongchun, Wang Mingpu, Sheng Xiaofei et al. *Journal of Alloys and Compounds*[J], 2013, 578: 208
- 9 Liu Shengdan, Li Chengbo, Han Suqi et al. *Journal of Alloys and Compounds*[J], 2015, 625: 34
- 10 Li Guirong, Cheng Jiangfeng, Wang Hongming et al. *Materials Research Express*[J], 2016, 3(10): 106 507
- 11 Urusovskaya A A, Alshits V I, Smirnov A E et al. *Crystallography Reports*[J], 2003, 48(5): 796
- 12 Jiang Chenxi, Wang Haiyan, Chen Xiangrong et al. *Electrochimica Acta*[J], 2013, 112: 535
- 13 Li X, Fautrelle Y, Ren Z. *Acta Materialia*[J], 2007, 55(4): 1377
- 14 Liu Yin, Wang Qiang, Liu Tie et al. *Journal of Alloys and Compounds*[J], 2014, 590: 110
- 15 Li Yang, Luo Zhen, Yan Fuyu et al. *Materials and Design*[J], 2014, 56: 1025
- 16 Wang Qiang, Liu Tie, Wang Kai et al. *ISIJ International*[J], 2010, 50: 1941
- 17 Buchachenko A L. *Journal of Experimental & Theoretical Physics*[J], 2006, 102: 795
- 18 Urusovskaya A A, Alshits V I, Smirnov A E et al. *Crystallography Reports*[J], 2003, 48: 796
- 19 Wang Hongming, Li Peisi, Zheng Rui et al. *Acta Phys Sin*[J], 2015(8): 295 (in Chinese)
- 20 Li Guirong, Wang Hongming, Li Peisi et al. *Acta Phys Sin*[J], 2015, 64(14): 148 102
- 21 Li Guirong, Xue Fei, Wang Hongming et al. *Chinese Physics B*[J], 2016, 25(10): 262
- 22 Li Guirong, Wang Hongming, Yuan Xueting. *Materials Letters*[J], 2013, 99: 50
- 23 Liu Shengdan, Zhang Xinming, You Jianghai et al. *Special Casting & Nonferrous Alloys*[J], 2006, 26(11): 696
- 24 Xiong Minghua, Yan Hongge, Su Bin et al. *Special Casting & Nonferrous Alloys*[J], 2012, 32(11): 1062
- 25 Wu S, Zhao H Y, Lu A L et al. *Tsinghua Science and Technology, Natural Science Edition*[J], 2002, 42(2): 147
- 26 Molotskii M, Fleurov V. *J Phys Chem B*[J], 2000, 104: 3812
- 27 Cai Yeqing, Sun Jinzhong, Liu Chengjie et al. *Journal of Iron and Steel Research*[J], 2015, 22(11): 1024
- 28 Zheng Ziqiao, Li Hongying, Mo Zhiming. *The Chinese Journal of Nonferrous Metals*[J], 2001, 11(5): 771
- 29 Bao Weiping, Xu Guangming, Ban Chunyan et al. *Acta Physica Sinica*[J], 2004, 53(6): 2024
- 30 Dixit M, Mishra R S, Sankaran K K. *Materials Science and Engineering A*[J], 2008, 478(1-2): 163

静磁场处理对7055铝合金显微组织和性能的影响

李桂荣, 程江峰, 王宏明, 李超群

(江苏大学, 江苏 镇江 212013)

摘要: 研究了不同静磁场强度对 7055 铝合金显微组织和力学性能的影响, 其中, 位错特征、相变、织构、拉伸性能、断口形貌和残余应力都用先进检测技术进行了分析。结果表明: 试样中的位错密度随着磁感应强度 B 的增加而呈上升趋势, 位错由原来的低能胞状向网络状转变; 此外, 磁场也促进了晶粒的细化和 η (MgZn_2) 向 η' 的转变, 这有益于材料综合性能的提高。当 $B=3\text{ T}$ 时, 磁场弱化了晶粒择优取向且重新调整了晶粒结构, 此时, 材料获得最优性能, 延伸率, 残余应力, 抗拉强度分别为 10.5%, 38 MPa, 555 MPa。断口形貌也通过扫描电镜进行了分析, 其特征与材料塑性增强一致。

关键词: 7055 铝合金; 位错特征; 显微组织; 力学性能; 静磁场

作者简介: 李桂荣, 女, 1970 年生, 博士, 教授, 江苏大学材料科学与工程学院, 江苏 镇江 212013, E-mail: liguirong@ujs.edu.cn